Antiferromagnetic superexchange mediated by a resonant surface state in Sn/Si(111)

Jun-Ho Lee,[1] Xiao-Yan Ren,[2] Yu Jia,[2] and Jun-Hyung Cho[1,2,*]

[1]*Department of Physics and Research Institute for Natural Sciences, Hanyang University, 17 Haengdang-Dong, Seongdong-Ku, Seoul 133-791, Korea*

[2]*Center for Clear Energy and Quantum Structures, and School of Physics and Engineering, Zhengzhou University, Zhengzhou 450052, China*

(Received 7 May 2014; revised manuscript received 28 July 2014; published 22 September 2014)

The Sn overlayer on the Si(111) surface has been considered as a prototypical system for exploring two-dimensional (2D) correlated physics on the triangular lattice. Most of the previous theoretical studies were based on the presumption that the surface state dominantly originates from Sn dangling-bond (DB) electrons, leading to a strongly correlated 2D electronic system. By contrast, our density-functional theory calculations show that the Sn DB state significantly hybridizes with Si substrate states to form a resonant state. The strong resonance between the Sn $5p_z$ and Si $3p_z$ orbitals facilitates the recently observed antiferromagnetic order through superexchange interactions, giving rise to a band-gap opening. It is thus demonstrated that the insulating ground state of Sn/Si(111) can be characterized as a Slater-type insulator via band magnetism.

DOI: 10.1103/PhysRevB.90.125439 PACS number(s): 75.30.Et, 73.20.At, 75.10.Lp, 75.70.Rf

I. INTRODUCTION

Two-dimensional (2D) electronic systems have provided a fundamental platform for exploring low-dimensional condensed matter physics [1–3]. In particular, the spin-1/2 antiferromagnet on a 2D triangular lattice has attracted much attention both theoretically and experimentally due to its exhibition of many exotic phenomena such as the formation of spin liquids [4–7], superconductivity [8,9], and Mott insulators [10,11]. To realize such a 2D electron system, epitaxial atom adsorption on semiconductor surfaces has been employed [1–3,12]. For example, the 1/3-monolayer adsorption of Sn atoms on the Si(111) surface produces the $\sqrt{3}\times\sqrt{3}$ phase, where Sn adatoms are located at the T_4 site [see Fig. 1(a)]. On the basis of a simple valence bond picture that the Sn adsorption saturates all the dangling bonds (DBs) of underlying Si surface atoms to leave a single DB per Sn atom, the Sn/Si(111) system has been considered as an ideal playground for investigating 2D correlated physics on the triangular lattice [1–3,12–25].

Earlier scanning tunneling microscopy (STM) experiments reported that the Sn/Si(111) surface exhibits the $\sqrt{3}\times\sqrt{3}$ periodicity down to 6 K [13]. Although there was a subtle debate whether the Sn atoms are vertically fluctuating or static [14], a more comprehensive study [15] with STM, scanning tunneling spectroscopy (STS), angle-resolved photoelectron spectroscopy (ARPES), and photoelectron diffraction at temperatures from 300 K to 5 K identified that the Sn layer is nearly flat while this surface becomes insulating below ~60 K. However, such an insulating ground state was not supported by previous density-functional theory (DFT) studies [16–18] with the local density approximation (LDA) or the generalized gradient approximation (GGA), which predicted a metallic ground state with a half-filled surface band [denoted as S in Fig. 2(a)] at the Fermi level. In order to resolve the incorrect prediction of LDA, Profeta and Tosatti [18] took into account an on-site Coulomb interaction (designated as Hubbard U) by means of the LDA + U scheme to predict the observed insulating ground state. Therefore, the Mott-Hubbard mechanism was proposed to account for the insulating nature of Sn/Si(111), but it has recently been refined by more rigorous theories [19,20]. Hansmann *et al.* [19] solved the low-energy effective Hamiltonian within the 2D triangular lattice model by using fully self-consistent combined GW and dynamical mean-field theory, and they pointed out the importance of long-range Coulomb interactions beyond the on-site Coulomb interaction to adequately describe the insulating behaviors of Sn/Si(111). Using the combination of LDA plus cluster many-body calculations with ARPES experiment, Li *et al.* [20] showed that the insulating ground state has the collinear antiferromagnetic (AFM) $2\sqrt{3}\times\sqrt{3}$ order with $\sqrt{3}\times\sqrt{3}$ structural symmetry rather than the 120° spiral magnetic configuration [see Fig. 1(b)]. The stabilization of such a collinear AFM order was accounted for by the inclusion of electron hopping up to next-nearest-neighbor Sn atoms in the presence of strong on-site Coulomb interaction. Thus, the insulating phase of Sn/Si(111) has so far been described by taking into account the Hubbard U together with long-range Coulomb interactions or longer-range electron hopping [18–20]. It is noticeable that these previous theories were implicitly based on the valence bond picture or the localized-electron picture where the well-separated S band in the Si bulk gap was presumed to dominantly originate from the Sn $5p_z$ orbitals.

By contrast, we here present the itinerant character of the S state due to a strong resonance between the Sn $5p_z$ orbitals and the Si substrate $3p_z$ orbitals. Such a delocalized feature may be associated with the self-interaction error (SIE) inherent to conventional DFT calculations with the LDA or GGA. Note that the SIE causes the electron density to artificially spread out because delocalization reduces the spurious self-repulsion of electrons [27,28]. Indeed, previous LDA and GGA calculations for Sn/Si(111) incorrectly predicted the ground state to be metallic [16–18]. Therefore, it is very challenging to examine how the correction of SIE properly predicts the observed insulating phase of Sn/Si(111).

In the present study, we perform the semilocal and hybrid DFT calculations to investigate the nature of the insulating phase of Sn/Si(111). We find that the correction of SIE with

*Corresponding author: chojh@hanyang.ac.kr

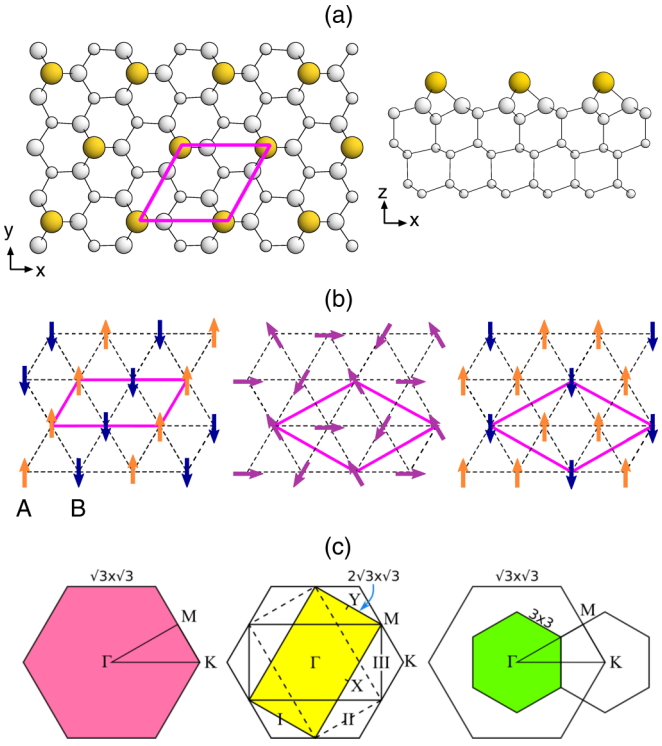

FIG. 1. (Color online) (a) Top (left) and side (right) views of the structure of Sn/Si(111). The dark and gray circles represent Sn and Si atoms, respectively. The Sn atom is located at a single threefold hollow site (T_4 site) above a second layer Si atom. The solid line indicates the $\sqrt{3}\times\sqrt{3}$ unit cell. The **x**, **y**, and **z** axes point along the $[11\bar{2}]$, $[1\bar{1}0]$, and [111] directions, respectively. Three different magnetic structures with the AFM, 120° spiral, and FI spin orders are schematically drawn in (b), where the corresponding $2\sqrt{3}\times\sqrt{3}$, 3×3, and 3×3 unit cells are indicated by the solid lines. The Brillouin zones (BZs) of various unit cells are drawn in (c). The rectangular I represents the BZ of the AFM structure shown in (b), while the rectangular II and III represent the BZs of other AFM spin alignments (see the Supplemental Material [26]).

the screened hybrid exchange-correlation functional of Heyd-Scuseria-Ernzerhof (HSE) [29,30] stabilizes the recently proposed AFM $2\sqrt{3}\times\sqrt{3}$ ground state with a band-gap opening. We show that this AFM spin ordering between far-separated (∼7 Å) Sn DB electrons is attributed to superexchange interactions mediated by the occupied and unoccupied resonating S states. The results suggest that the observed insulating phase of Sn/Si(111) [20] can be represented as a Slater-type insulator [31] via itinerant magnetism, not by a Mott-type insulator [15,17–20] driven by strong electron correlations within the 2D Sn overlayer.

II. CALCULATIONAL METHODS

The present semilocal and hybrid DFT calculations were performed using the FHI-AIMS [32] code for an accurate, all-electron description based on numeric atom-centered orbitals, with "tight" computational settings. For the exchange-correlation energy, we employed the GGA functional of Perdew-Burke-Ernzerhof (PBE) [33] and the hybrid functional of HSE [29,30] given by

$$E_{\rm XC}^{\rm HSE} = \alpha E_X^{\rm HF,SR}(\omega) + (1-\alpha)E_X^{\rm PBE,SR}(\omega) + E_X^{\rm PBE,LR}(\omega) + E_C^{\rm PBE}. \quad (1)$$

Here, the mixing factor $\alpha(=0.25)$ controls the amount of exact Fock exchange energy and the screening parameter $\omega(=0.11\ \text{bohr}^{-1})$ defines the separation of short range (SR) and long range (LR) for the exchange energy. The Si(111) substrate [with the optimized lattice constant $a_0 = 5.482$ (5.452) Å for the PBE (HSE) calculation] was modeled by a periodic slab geometry consisting of the ten-layer slab with ∼34 Å of vacuum in between the slabs. Here, each Si atom in the bottom layer was passivated by one H atom. The **k**-space integrations for the nonmagnetic (NM), AFM, and ferrimagnetic (FI) structures were done with the 15×15, 9×18, and 9×9 uniform meshes in the surface Brillouin zones of the $\sqrt{3}\times\sqrt{3}$, $2\sqrt{3}\times\sqrt{3}$, and 3×3 unit cells, respectively. All atoms except the bottom four layers were allowed to relax along the calculated forces until all the residual force components were less than 0.02 eV/Å.

III. RESULTS

We first study the electronic structure of the NM $\sqrt{3}\times\sqrt{3}$ structure using the PBE functional. The optimized NM structure is displayed in Fig. 1(a), and its band structure exhibits the presence of a half-filled S band [see Fig. 2(a)] crossing the Fermi level E_F. In order to examine the nature of the S state, we calculate the angular-momentum resolved partial density of states (DOS) for each atom. Figure 2(b) shows that near E_F the partial DOS projected onto the Sn $5p$ orbitals only amounts

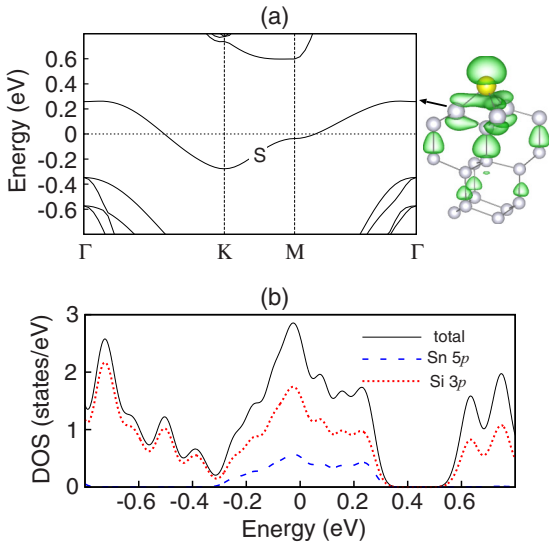

FIG. 2. (Color online) (a) Surface band structure and (b) DOS of the NM $\sqrt{3}\times\sqrt{3}$ structure obtained using the PBE functional. The band dispersions are plotted along the symmetry lines of the Brillouin zone of the $\sqrt{3}\times\sqrt{3}$ unit cell. The charge character of the S state at the Γ point is also shown with an isosurface of 0.004 e/Å^3. The energy zero represents the Fermi level. In (b), the total DOS, Sn $5p$ partial DOS, and Si $3p$ partial DOS are displayed with solid, dashed, and dotted lines, respectively.

TABLE I. Calculated total energies (in meV per $\sqrt{3}\times\sqrt{3}$ unit cell) of the AFM, FI, and FM structures relative to the NM structure obtained using the HSE and HSE + vdW schemes.

	AFM	FI	FM
HSE	−65.1	−64.2	−47.9
HSE+vdW	−62.6	−61.4	−45.2

to ∼35% of that projected onto the Si $3p$ orbitals, indicating a strong hybridization between the two orbitals. As shown in the inset of Fig. 2(a), the charge character of the S state represents the significant hybridization of the Sn $5p_z$ orbital with the Si substrate $3p_z$ orbitals, giving rise to a large delocalization up to the fifth deeper Si substrate layer. This resonant character of the S state was overlooked in the previously proposed Mott-type mechanism [17–20] where the S state was presumed to have a localized-electron character, mostly originating from the Sn $5p_z$ orbitals. In order to find the insulating phase observed below ∼60 K [15], we also performed the spin-polarized PBE calculations for several magnetic structures such as the AFM $2\sqrt{3}\times\sqrt{3}$, FI 3×3, and ferromagnetic (FM) $\sqrt{3}\times\sqrt{3}$ structures, but we were unable to find the stabilization of any spin ordering.

To circumvent the possible SIE inherent in the PBE calculation, we use the HSE functional to optimize the NM $\sqrt{3}\times\sqrt{3}$ structure as well as various magnetic structures. We find that the AFM, FI, and FM structures become more stable than the NM structure by $\Delta E_{\text{NM-AFM}} = 65.1$, $\Delta E_{\text{NM-FI}} = 64.2$, and $\Delta E_{\text{NM-FM}} = 47.9$ meV per $\sqrt{3}\times\sqrt{3}$ unit cell, respectively [34] (see Table I). Here, the AFM structure is slightly more stable than the FI structure by ∼1 meV, and the comparison of the calculated band structures with a recent ARPES experiment [35] carried out at a low temperature of 18 K supports the AFM ground state, as discussed below. In the optimized AFM structure, two Sn atoms in the $2\sqrt{3}\times\sqrt{3}$ unit cell are at the same height, indicating a $\sqrt{3}\times\sqrt{3}$ structural symmetry as determined from x-ray diffraction data [13]. Assuming that the insulating AFM structure has a negligible entropy arising from the spin and electron degrees of freedom [18] while the metallic NM structure has an electronic entropy of γT (where γ is the electronic specific heat coefficient), we obtain the entropy-related free energy difference ($T\Delta S$) between the AFM and NM structures. Hence, if we use $\gamma \approx 0.1$ meV/site K^2 taken by Profeta and Tosatti [18,36], we can roughly estimate a metal-insulator transition temperature of ∼25 K from the AFM to the NM structure, well comparable with the experimentally measured [15] value of ∼60 K.

To examine the influence of van der Waals (vdW) interactions on the energetics, we use the HSE + vdW scheme [37] where the vdW coefficient and radii are determined using the self-consistent electron density. The calculated HSE + vdW total energies of the AFM, FI, and FM structures relative to the NM structure are also listed in Table I. We find that the AFM structure is still more stable than the FI structure by $\Delta E_{\text{FI-AFM}} = 1.2$ meV, slightly larger than that (0.9 meV) obtained using the HSE scheme. Thus, the inclusion of vdW interactions within the HSE + vdW scheme does not reverse the stability of the AFM and FI structures.

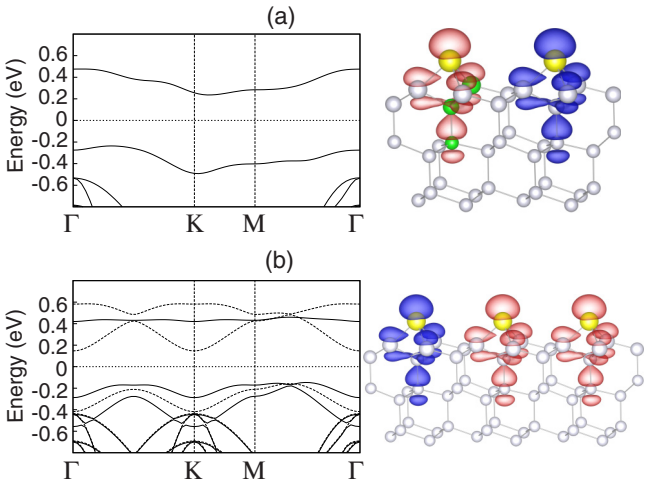

FIG. 3. (Color online) Surface band structures and spin densities of the (a) AFM and (b) FI structures obtained using the HSE functional. The spin-up (spin-down) density is drawn in bright (dark) color with an isosurface of 0.01 (−0.01) e/Å^3. The dark circles in (a) indicate Si_1 atoms in the first, second, and third Si layers (see Table I). In (b), the spin-up (spin-down) band is displayed with the solid (dashed) line.

Figures 3(a) and 3(b) show the calculated band structures for the AFM and FI structures, respectively. Compared to the FI structure, the AFM structure shows better agreement with a recent ARPES data [see Fig. 1S(a) of the Supplemental Material [26]] of Li *et al.* [20]. The somewhat broad ARPES dispersion of the S band may be due to the presence of three different domains with degenerate AFM spin orientations. Note that there are three different spin orientations of the AFM $2\sqrt{3}\times\sqrt{3}$ structure due to its threefold rotation symmetry. We find that the dispersions of the S band along Γ-K-M-Γ is slightly different depending on the spin orientation, but all three dispersions are well within the ARPES measurement [see Fig. 3(a) and Fig. 1S of the Supplemental Material [26]]. From the calculated band structure along Γ-Y-M-X-Γ (see Fig. 2S of the Supplemental Material [26]), we obtain a band gap of 328 meV. This value is much larger than the experimental value of ∼40 meV estimated from STS [15], but closer to that (∼200 meV) observed by ARPES [35]. In order to examine how α influences the band gap of the AFM state, we perform the HSE calculations as a function of α. We find that the band gap is opened above $\alpha \approx 0.1$ and it increases monotonically with increasing α. As a result, the HSE calculation with $\alpha \approx 0.2$ reproduces well the observed [35] band gap of 0.2 eV. It is noticeable that the three degenerate AFM spin configurations exhibit a band energy offset of ∼0.2 eV between the Γ and K points, consistent with the ARPES data of ∼0.1 eV [20]. On the other hand, the FI structure with the 3×3 unit cell shows a degenerate band energy at the Γ and K points, both of which are equivalent to each other through band back-folding. As pointed out by Li *et al.* [20], such a symmetric band-dispersion feature of the 3×3 magnetic structure along Γ-K was used to rule out the 120° spiral spin order [Fig. 1(b)].

TABLE II. Calculated spin moments (in μ_B) of Sn and Si atoms in the AFM structure. The spin moment of each atom is calculated using Mulliken analysis. Each Si layer is composed of three Si atoms below the site A (or B), where Si_1 is indicated with the dark circles in Fig. 3(a).

Sn		A site			B site	
		0.253			−0.253	
Si layer	Si_1	Si_2	Si_3	Si_1'	Si_2'	Si_3'
First	0.122	0.127	0.127	−0.122	−0.127	−0.127
Second	0.025	0.000	0.000	−0.025	0.000	0.000
Third	0.137	0.006	0.006	−0.137	−0.006	−0.006
Fourth	0.003	0.003	0.003	−0.003	−0.003	−0.003

The resonant character of the S state is also reflected in the calculated spin density that exhibits a penetration up to the fourth deeper Si atomic layers [see Figs. 3(a) and 3(b)]. Using a Mulliken population analysis, we obtain the spin moments m of Sn and Si atoms in each layer. The calculated spin moments for the AFM structure are given in Table II. We find that the Sn atom has $m \approx \pm 0.25\mu_B$, while the Si atoms in the first and third substrate layers have m as large as $\sim\pm 0.13\mu_B$. These values are significantly larger than those for Si atoms in the second and fourth Si layers (see Table II). Our finding of such a large spin delocalization due to surface resonance corresponds to an itinerant magnetism, contrasting with the localized magnetism in the previously proposed Mott-Hubbard mechanism [18] where each Sn atom has a localized spin moment of $\sim 1\mu_B$ arising from the DB electron.

To understand the microscopic mechanism for the AFM spin ordering, we plot the spin-polarized local DOS projected onto the Sn atom [A or B site in Fig. 1(b)] in Fig. 4, together with their spin characters. It is seen that the occupied (unoccupied) spin-up and spin-down S states are localized at the A (B) and B (A) sites, respectively. Since electronic states with the same spin direction can hybridize with each other, the hybridization takes place between the occupied and unoccupied spin-up (spin-down) states localized at the A (B) and B (A) sites, respectively, yielding not only an energy gain from the exchange kinetic energy but also the formation of an insulating gap [38]. This kind of exchange interaction mediated by two electronic states which are energetically separated well below and above the Fermi level is characterized as a superexchange mechanism [39,40]. It is likely that such a superexchange interaction can be facilitated due to the considerable hybridization of the Sn $5p_z$ orbitals with the Si $3p_z$ orbitals.

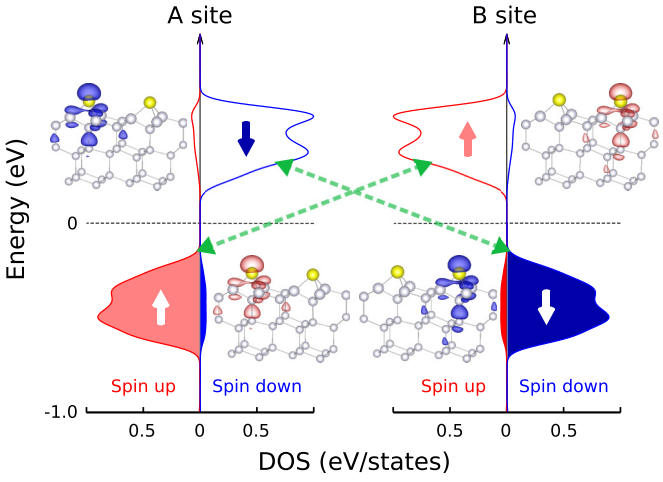

FIG. 4. (Color online) Spin-polarized local DOS at the Sn atom of the AFM structure. The A (B) site indicates the Sn atom with the up (down) spin [see Fig. 1(b)]. The charge characters of the spin-up and spin-down states for the highest occupied and the lowest unoccupied band are taken at the Γ point with an isosurface of 0.005 e/Å^3.

Most of the previous theoretical studies [18–20] for the insulating phase of Sn/Si(111) have taken into account electronic correlation effects within the Sn overlayer based on the localized-electron picture where the DB electrons are dominantly localized at Sn atoms and therefore the low-energy effective Hamiltonians are constructed on the 2D Sn lattice. However, this treatment of a strongly correlated 2D electronic system seems inappropriate to simulate the Sn overlayer on Si(111) that involves the resonating DB state. Obviously, near E_F the local DOS at the first, second, and third Si-layer atoms are comparable to that at the Sn atoms (see Fig. 3S in the Supplemental Material [26]). Such a delocalized character of the S state makes electronic correlation effects weakened, thereby unlikely to be represented as Mott-type insulator. Instead, the present magnetically driven insulating phase with an itinerant single-particle approach can be represented as a Slater-type insulator.

Finally, it is noteworthy that both Sn/Si(111) and Sn/Ge(111) [41] have an identical AFM ground state which is more stable than the NM structure by 62.6 and 40.6 meV, respectively, obtained using the HSE + vdW scheme. This result indicates that the AFM ordering in Sn/Si(111) would be stronger than that in Sn/Ge(111), consistent with the experimental evidence that Sn/Si(111) has a larger metal-insulator transition temperature of ∼60 K compared to that (∼30 K) in Sn/Ge(111). Here, the relatively weaker AFM order in Sn/Ge(111) may be associated with the fact that the resonant character of the S state in Sn/Ge(111) can be more dominant because the Ge $4p$ orbitals are spatially more extended compared to the Si $3p$ orbitals due to the presence of the additional d electrons in Ge.

IV. SUMMARY

To conclude, unlike the semilocal DFT calculation predicting a metallic NM $\sqrt{3}\times\sqrt{3}$ ground state, the hybrid DFT calculation correctly predicted the insulating AFM $2\sqrt{3}\times\sqrt{3}$ ground state which was recently proposed by ARPES [20]. We identified the resonant character of the Sn DB state due to a strong hybridization between the Sn $5p_z$ and Si $3p_z$ orbitals, leading to the facilitation of an AFM ordering through superexchange interactions. The resulting significant spin delocalization over Sn atoms and Si substrate atoms corresponds to an itinerant magnetism, contrasting with a localized magnetism inherent in the Mott-type mechanism. Therefore, our results demonstrated that the insulating phase of Sn/Si(111) can be characterized as a Slater-type insulator via

band magnetism. It is notable that several metal overlayers on semiconductor surfaces such as alkali adatoms on GaAs(110) and K adatoms on B-doped Si(111) were reported to exhibit the insulating ground state caused by strong electron correlations [42]. However, we anticipate that such quasi-2D systems would have the resonant character of the surface state that plays an important role in forming an insulating gap through AFM superexchange.

ACKNOWLEDGMENTS

This work was supported by a National Research Foundation of Korea (NRF) grant funded by the Korea Government (MSIP) (Grant No. 2014M2B2A9032247). The calculations were performed by KISTI supercomputing center through the strategic support program (KSC-2013-C3-032) for the supercomputing application research.

[1] J. M. Carpinelli, H. H. Weitering, E. W. Plummer, and R. Stumpf, Nature (London) **381**, 398 (1996).
[2] J. M. Carpinelli, H. H. Weitering, M. Bartkowiak, R. Stumpf, and E. W. Plummer, Phys. Rev. Lett. **79**, 2859 (1997).
[3] H. H. Weitering, J. M. Carpinelli, A. V. Melechko, J. Zhang, M. Bartkowiak, and E. W. Plummer, Science **285**, 2107 (1999).
[4] L. Balent, Nature (London) **464**, 199 (2010).
[5] Z. Y. Meng, T. C. Lang, S. Wessel, F. F. Assaad, and A. Muramatsu, Nature (London) **464**, 847 (2010).
[6] P. W. Anderson, Mater. Res. Bull. **8**, 153 (1973).
[7] R. Coldea, D. A. Tennant, A. M. Tsvelik, and Z. Tylczynski, Phys. Rev. Lett. **86**, 1335 (2001).
[8] P. W. Anderson, Science **235**, 1196 (1987).
[9] T. Zhang, P. Cheng, W.-J. Li, Y.-J. Sun, G. Wang, X.-G. Zhu, K. He, L. Wang, X. Ma, X. Chen, Y. Wang, Y. Liu, H.-Q. Lin, J.-F. Jia, and Q.-K. Xue, Nat. Phys. **6**, 104 (2010).
[10] Y. Shimizu, K. Miyagawa, K. Kanoda, M. Maesato, and G. Saito, Phys. Rev. Lett. **91**, 107001 (2003).
[11] Y. Kurosaki, Y. Shimizu, K. Miyagawa, K. Kanoda, and G. Saito, Phys. Rev. Lett. **95**, 177001 (2005).
[12] E. Tosatti, in *Electronic Surface and Interface States on Metallic Systems*, edited by E. Bertel and M. Donath (World Scientific, Singapore, 1995), p. 67.
[13] H. Morikawa, I. Matsuda, and S. Hasegawa, Phys. Rev. B **65**, 201308(R) (2002).
[14] S. Colonna, F. Ronci, A. Cricenti, and G. Le Lay, Phys. Rev. Lett. **101**, 186102 (2008).
[15] S. Modesti, L. Petaccia, G. Ceballos, I. Vobornik, G. Panaccione, G. Rossi, L. Ottaviano, R. Larciprete, S. Lizzit, and A. Goldoni, Phys. Rev. Lett. **98**, 126401 (2007).
[16] F. Flores, J. Ortega, R. Pérez, A. Charrier, F. Thibaudau, J. M. Debever, and J. M. Themlin, Prog. Surf. Sci. **67**, 299 (2001).
[17] S. Schuwalow, D. Grieger, and F. Lechermann, Phys. Rev. B **82**, 035116 (2010).
[18] G. Profeta and E. Tosatti, Phys. Rev. Lett. **98**, 086401 (2007).
[19] P. Hansmann, T. Ayral, L. Vaugier, P. Werner, and S. Biermann, Phys. Rev. Lett. **110**, 166401 (2013).
[20] G. Li, P. Höpfner, J. Schäfer, C. Blumenstein, S. Meyer, A. Bostwick, E. Rotenberg, R. Claessen, and W. Hanke, Nat. Commun. **4**, 1620 (2013), and references therein.
[21] G. Santoro, S. Scandolo, and E. Tosatti, Phys. Rev. B **59**, 1891 (1999).
[22] G. Li, M. Laubach, A. Fleszar, and W. Hanke, Phys. Rev. B **83**, 041104(R) (2011).
[23] G. Profeta, A. Continenza, L. Ottaviano, W. Mannstadt, and A. J. Freeman, Phys. Rev. B **62**, 1556 (2000).
[24] A. Charrier, R. Pérez, F. Thibaudau, J.-M. Debever, J. Ortega, F. Flores, and J.-M. Themlin, Phys. Rev. B **64**, 115407 (2001).
[25] G. Ballabio, S. Scandolo, and E. Tosatti, Phys. Rev. B **61**, R13345(R) (2000).
[26] See Supplemental Material at http://link.aps.org/supplemental/10.1103/PhysRevB.90.125439 for the band structure and the local DOS of the AFM $2\sqrt{3}\times\sqrt{3}$ structure computed using the HSE functional.
[27] A. J. Cohen, P. Mori-Sánchez, and W. Yang, Science **321**, 792 (2008).
[28] P. Mori-Sánchez, A. J. Cohen, and W. Yang, Phys. Rev. Lett. **100**, 146401 (2008).
[29] J. Heyd, G. E. Scuseria, and M. Ernzerhof, J. Chem. Phys. **118**, 8207 (2003).
[30] A. V. Krukau, O. A. Vydrov, A. F. Izmaylov, and G. E. Scuseria, J. Chem. Phys. **125**, 224106 (2006).
[31] J. C. Slater, Phys. Rev. **82**, 538 (1951).
[32] V. Blum, R. Gehrke, F. Hanke, P. Havu, V. Havu, X. Ren, K. Reuter, and M. Scheffler, Comput. Phys. Commun. **180**, 2175 (2009).
[33] J. P. Perdew, K. Burke, and M. Ernzerhof, Phys. Rev. Lett. **77**, 3865 (1996); **78**, 1396(E) (1997).
[34] It was found that changing the basis set from a light setting to a tight one changes $\Delta E_{\text{FI-AFM}}$ by an increase of 0.35 meV, increasing the k-point sampling from $9\times9\times1$ ($9\times18\times1$) to $12\times12\times1$ ($12\times24\times1$) for the FI (AFM) structure changes $\Delta E_{\text{FI-AFM}}$ by an increase of 0.19 meV, and increasing the Si slab thickness from 10 layers to12 layers changes $\Delta E_{\text{FI-AFM}}$ by an increase of 0.26 meV. These results indicate that more rigorous calculation parameters increase the stability of the AFM structure relative to the FI structure.
[35] P. Höpfner, Ph.D. thesis, Universität Würzburg, 2012.
[36] K. Kanoda, J. Phys. Soc. Jpn. **75**, 051007 (2006).
[37] A. Tkatchenko and M. Scheffler, Phys. Rev. Lett. **102**, 073005 (2009).
[38] K. Sato, L. Bergqvist, J. Kudrnovsky, P. H. Dederichs, O. Eriksson, I. Turek, B. Sanyal, G. Bouzerar, H. Katayama-Yoshida, V. A. Dinh, T. Fukushima, H. Kizaki, and R. Zeller, Rev. Mod. Phys. **82**, 1633 (2010).
[39] J. B. Goodenough, Phys. Rev. **100**, 564 (1955).
[40] J. Kanamori, J. Phys. Chem. Solids **10**, 87 (1959).
[41] J.-H. Lee, H.-J. Kim, and J.-H. Cho, Phys. Rev. Lett. **111**, 106403 (2013); in this paper, we predicted the FI ground state for Sn/Ge(111). After the publication of Ref. [20] that reported the experimental evidence of the AFM ground state for Sn/Si(111), we performed the HSE + vdW calculation for the AFM structure of Sn/Ge(111) and found that the AFM structure is more stable than the FI state by 2.9 meV.
[42] A. Tejeda, Y. Fagot-Révurat, R. Cortés, D. Malterre, E. G. Michel, and A. Mascaraque, Phys. Status Solidi A **209**, 614 (2012), and references therein.